Evaluation of photoelectric processes in photorefractive crystals via the exposure characteristics of light diffraction

2005 J. Phys.: Condens. Matter 17 33

(http://iopscience.iop.org/0953-8984/17/1/004)

INSTITUTE OF PHYSICS PUBLISHING JOURNAL OF PHYSICS: CONDENSED MATTER

J. Phys.: Condens. Matter **17** (2005) 33–41 doi:10.1088/0953-8984/17/1/004

Evaluation of photoelectric processes in photorefractive crystals via the exposure characteristics of light diffraction

A Kadys, V Gudelis, M Sudzius and K Jarasiunas

Department of Semiconductor Optoelectronics, Institute of Materials Science and Applied Research, Vilnius University, Sauletekio avenue 9, Building 3, LT-10222 Vilnius, Lithuania

E-mail: markas.sudzius@ff.vu.lt

Received 29 July 2004, in final form 1 November 2004
Published 10 December 2004
Online at stacks.iop.org/JPhysCM/17/33

Abstract

We demonstrate a novel way to analyse carrier recombination and transport processes in photorefractive semiconductors via the exposure characteristics of light induced diffraction. The results of a picosecond four-wave mixing on free carrier gratings in semi-insulating GaAs crystals at various grating periods and modulation depths of a light interference pattern are discussed. The role of a deep-trap recharging in carrier diffusion and recombination is sensitively revealed through a feedback effect of a space–charge field to non-equilibrium carrier transport.

1. Introduction

Spatial modulation of non-equilibrium carriers created by a light interference field leads to a refractive index modulation, on which the delayed probe beam is diffracted and monitors the carrier dynamics. In photorefractive semiconductors, when carriers are excited from deep impurity levels, the transport and trapping create a space–charge (SC) field along the grating vector. This leads to peculiarities in the non-equilibrium carrier transport, e.g. competition of diffusion and drift of major carriers [1], which strongly depends on the excitation conditions. To a large extent these peculiarities are determined by gradual changes of carrier generation mechanisms with increasing excitation energy [2]. Therefore, the processes of carrier generation and transport in a spatially-modulated internal electric field have to be considered explicitly for the evaluation of the parameters of semi-insulating photorefractive crystals.

Our recent studies of non-equilibrium carrier dynamics in semi-insulating CdTe crystals with different compensation ratios of deep impurity have shown a strong influence of the charge state of the deep impurity on non-equilibrium carrier generation and transport in the subnanosecond time domain [2]. Numerical analysis has revealed a way to determine the dominant type of photoexcited carriers in a crystal after its complex codoping. In particular,

it was shown that the increase or decrease of effective diffusion coefficient D with excitation can be used as a criterion to distinguish the type of photogenerated carriers.

In this paper we extend the applicability of a degenerate four-wave mixing (DFWM) technique for the characterization of the photoelectric properties of photorefractive GaAs. In addition to more common measurements of grating decay kinetics, we analyse the diffraction efficiency as a function of excitation energy measured at various times after the photoexcitation of the crystal by a short laser pulse. The technique is applied for the analysis of deep impurity related carrier generation, diffusion, recombination, space charge field formation and its feedback to carrier transport in GaAs at 300 K.

2. Transient free carrier grating characteristics

Optical illumination of GaAs at $\lambda = 1.06$ μm (i.e. in the spectral region $E_g/2 < h\nu < E_g$) leads to a change of its refractive index via free-carrier (FC) nonlinearity which is described by the Drude–Lorentz model [3, 4]:

$$\Delta n_{FC} = -(e^2/2n_0w^2\epsilon_0)(\Delta n/m_e^* + \Delta p/m_h^*), \tag{1}$$

where $\Delta n/m_e^*$ and $\Delta p/m_h^*$ are the modulated concentrations of electrons and holes normalized to their effective masses, and n_0 is the refractive index of the crystal at the frequency w of the probe beam. The diffraction efficiency of such a grating can be described as

$$\eta = I_1/I_T \approx (\pi \Delta n_{FC} d/\lambda)^2, \tag{2}$$

where I_1 and I_T are the diffracted and transmitted intensities of the probe beam, d is the sample thickness and λ is the wavelength of the probe beam. At 1.06 μm wavelength, the optical cross-section for the transitions from the valence band to $EL2^+$ (ionized EL2 centres) is much smaller than that for the transitions from $EL2^0$ (neutral EL2 centres) to the conduction band [5]. Therefore, assuming that the concentration of ionized EL2 centres N^+ is much lower than the concentration of neutral EL2 centres N_0, the absorption at 1.06 μm is typically attributed to the photoionization of $EL2^0$.

The exposure characteristics (EC) of diffraction efficiency (i.e. the diffraction efficiency as a function of excitation energy) were shown to be very informative if carrier generation mechanisms have to be characterized [6–9]. For relatively low efficiencies, the exposure characteristic of a diffracted signal follows a power law dependence [6, 10]. Assuming that the carrier concentration increases with excitation as $n \propto I^\gamma$, according to (2), the diffraction efficiency of the grating will increase as $\eta \propto I^{2\gamma}$. In a general case, a linear carrier generation ($\gamma = 1$) leads to $\eta \propto I^2$, while a two-photon light absorption ($\gamma = 2$) may increase the slope of the EC up to $\eta \propto I^4$.

During simultaneous recording and probing of the transient gratings by subnanosecond pulses, the behaviour of the EC in GaAs is essentially determined by the peculiarities of carrier generation [11]. At later times, however, this dependence is inevitably modified by carrier recombination and diffusion. The extent to which these processes influence the EC behaviour is determined by characteristic time constants of recombination and diffusion (τ_R and τ_D respectively) and the probe beam delay time Δt. The time constants τ_R and τ_D define the carrier grating decay time, $1/\tau_G = 1/\tau_R + 1/\tau_D$. However, since $\tau_D \propto \Lambda^2$, it is easy to achieve either the diffusion or recombination process becoming dominant by varying the grating period Λ. In semi-insulating crystals, in the case when photocarriers are excited from the midgap states, both τ_R and τ_D depend strongly on the excitation energy. This feature as well as the impact of the SC field on photocarrier transport can be sensitively traced by changes in the characteristic slope coefficients of the EC at various excitations and delay times of the probe beam.

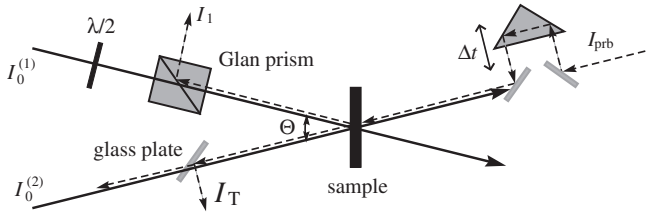

Figure 1. Optical scheme of experimental setup.

3. Sample and technique

The laser source for our experiments was a mode-locked Nd:YAG laser. The average pulse width was 27 ps FWHM and the beam diameters at the sample were ≈1.4 mm FWHM. The pulse was divided into two s-polarized parts of the signal (with intensities $I_0^{(1)}$ and $I_0^{(2)}$) which recombined at an angle Θ to produce a grating with period of $\Lambda = \lambda/[2\sin(\Theta/2)]$ in the crystal (see figure 1). The modulation depth of the light interference pattern $m = 2\sqrt{I_0^{(1)} I_0^{(2)}}/(I_0^{(1)} + I_0^{(2)})$ was controlled by the polarization state of $I_0^{(1)}$. The temporal decay of the free carrier grating and its dependence on the overall light intensity $I_0 = I_0^{(1)} + I_0^{(2)}$ is studied by directing a p-polarized probe I_{prb} (with at least one order of magnitude lower intensity than that of the recording ones) to the same spot on the sample, which Bragg diffracts and counterpropagates to the $I_0^{(1)}$ beam. A Glan polarizer oriented to reflect p-polarization is used for separation of the diffracted beam I_1.

Our experiments were performed using a GaAs crystal grown by the liquid-encapsulated Czochralski (LEC) technique. The sample was cut from the central part of a 3 in. diameter GaAs substrate (In-alloyed to minimize the dislocation density) with a dark resistivity $\rho = 5 \times 10^6\ \Omega$ cm and dislocation density $N_D \approx 3 \times 10^4\ \text{cm}^{-2}$. Some of the optical and electrical properties of this sample have been investigated by ns-DFWM and are reported in [12, 13]. In particular, it was shown by comparison of experimentally measured and calculated kinetics that the dark-state compensation of the crystal by EL2 $R = N_{imp}/N_T = N^+/(N_0 + N^+) \approx 0$, where N_{imp} is the net concentration of shallow impurities and N_T is the total concentration of EL2 centres [12].

In order to assist the qualitative analysis of the experimental results, we solve numerically a set of material equations (rate equations for electrons, holes, $EL2^+$, and Poisson equation [2, 14]) by means of the method of finite elements. The system of partial differential equations is coupled to the equation for the light interference pattern $I(x,t) = I_0 f(t)[1 + m\cos(K_g x)]$ with I_0 as the light intensity, m as the modulation depth of the interference fringes, and $K_g = 2\pi/\Lambda$ as the grating vector. $f(t)$ is the normalized Gaussian function with FWHM equal to the laser pulse duration τ_L.

Our model takes into account EL2 photoionization (photoionization cross-section S_e for the electrons and S_h for the holes), recombination of carriers to the $EL2^0$ and $EL2^+$ states (recombination coefficient γ_e and γ_h respectively), band-to-band two-photon absorption (absorption coefficient β), and bimolecular recombination of electron–hole pairs (recombination coefficient γ_{eh}). Table 1 gives a list of the parameters used in the calculations.

4. Results and discussion

4.1. Grating decay kinetics

In the first instance, we discuss the excitation-dependent kinetics of the diffraction efficiency in order to identify the experimental conditions which are most favorable to reveal the peculiarities of carrier recombination and transport via the exposure characteristics. In figure 2, we show the

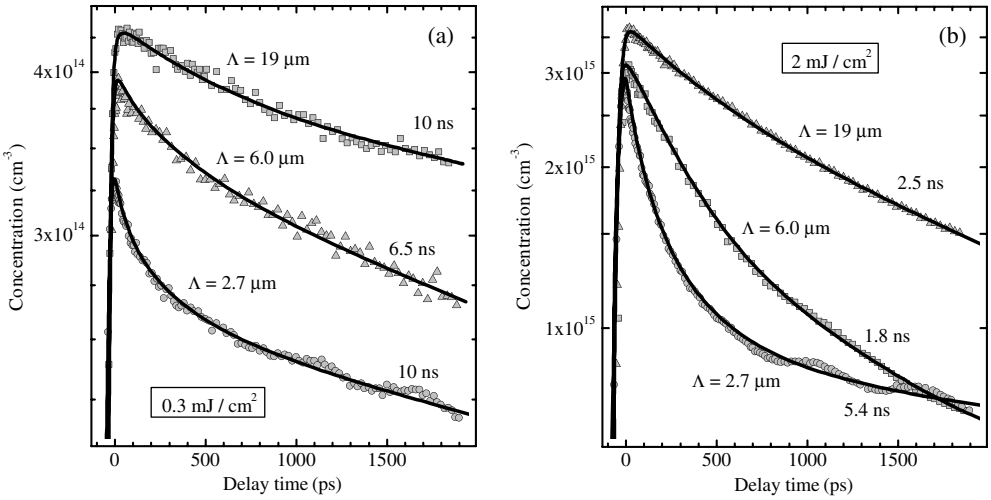

Figure 2. Dynamics of free carrier gratings measured at different grating periods and two excitation levels. The time values given indicate the characteristic grating decay times τ_G. The thick solid curves are to guide the eye.

Table 1. Crystal parameters used in the calculations.

Parameter	Value	Reference
Total EL2 defect density, N_T	1×10^{16} cm^{-3}	[15]
Crystal compensation ratio by EL2, R	0	[12, 13]
Electron photoionization cross-section, S_n at 1.06 μm	1×10^{-16} cm^2	[16]
Hole photoionization cross-section, S_p at 1.06 μm	3×10^{-17} cm^2	[17]
Two-photon absorption coefficient, β at 1.06 μm	25 cm GW^{-1}	[18]
Electron recombination coefficient, γ_n	1.3×10^{-7} cm^3 s^{-1}	This work
Hole recombination coefficient, γ_p	3.3×10^{-11} cm^3 s^{-1}	[19]
Bimolecular recombination coefficient, γ_{np}	1×10^{-10} cm^3 s^{-1}	[20]
Electron mobility, μ_n	5000 cm^2 V^{-1} s^{-1}	[21, 22]
Hole mobility, μ_p	400 cm^2 V^{-1} s^{-1}	[21, 22]
Effective mass of electrons, m_e^*	0.063	[21]
Effective mass of holes, m_h^*	0.51	[21]
Relative permittivity, ε_r	13.2	[23]

kinetics of photoexcited carrier modulation at different grating periods and excitation energies. The instantaneous values of carrier concentration were recalculated from the experimentally measured diffraction efficiencies using equations (1) and (2). In the calculation, we have neglected the contribution from holes since in our experiments the photocarriers are excited mainly from neutral EL2 states [12]. Moreover, according to equation (1), the contribution of holes to the refractive index modulation is $m_h^*/m_e^* \approx 8$ times lower than that of the electrons. Thus the carrier concentration in figure 2 corresponds to the electron concentration.

Grating decay kinetics in the subnanosecond or a few nanoseconds time domain provide transients of carrier relaxation, which are affected by some coexisting and interrelated non-equilibrium processes after excitation by a short picosecond pulse. Varying with time, the grating decay rate reflects the dynamics of the carrier density, the formation of the space–charge field, and its feedback to carrier transport, and results in non-exponential grating decay, especially pronounced at small grating periods. The carrier transport becomes dependent on

the carrier density, as the origin of the SC changes with excitation (i.e. from the SC field between mobile carriers and ionized deep impurities to the Dember field between mobile carriers). At small grating periods (2.7 μm), the electron diffusion dominates in the grating decay ($\tau_D \propto \Lambda^2$), but electron spatial redistribution creates the SC field which efficiently opposes the diffusive current. As a consequence, the grating decay time is prolonged to 10 ns (at low excitations, figure 2(a)) and 5.4 ns (at higher excitations, figure 2(b)) at $\Delta t > 1$ ns.

In contrast, at large grating periods, the SC field is relatively weak ($E_{SC} \propto 1/\Lambda$); therefore, the process of electron recombination to the EL2$^+$ states is solely dominant. The concentration of photoexcited electrons is roughly the same as the number of EL2$^+$ states ($n \approx N^+$) since, for our sample, all the EL2 states are filled by electrons in the dark state [12]. Consequently, the FC grating decays due to the capture of electrons by EL2$^+$ states with $\tau_G \approx \tau_R = 1/(\gamma_n N^+)$ characteristic decay time, whereas the non-exponential character of the kinetics reflects the fact that N^+ is time dependent. That also explains the significantly faster grating decay at 2 mJ cm^{-2} ($\tau_G = 2.5$ ns, figure 2(b)) than that at 0.3 mJ cm^{-2} ($\tau_G = 10$ ns, figure 2(a)), which is due to the increasing number of EL2$^+$ states with excitation energy. Assuming that $N_T = 1 \times 10^{16}$ cm^{-3}, the electron recombination coefficient $\gamma_n = 1.3 \times 10^{-7}$ cm^3 s^{-1} is required in order to describe the experimentally measured decrease of grating decay time τ_G with excitation at $\Delta t > 1$ ns and $\Lambda = 19$ μm.

The grating decay kinetics at an intermediate period ($\Lambda = 6$ μm in our experiments) provides transients of the grating decay, when diffusion, drift, and recombination contribute simultaneously to the carrier modulation and do not allow us to observe either diffusion or recombination governed grating decay in the used time domain of 2 ns. This leads to a gradual decrease of the grating decay rate with time due to the rather weak SC field at this grating period.

The analysis of grating decay dynamics shows that the interpretation of non-exponential decay transients in the presence of an SC field is possible (although very qualitative) either at relatively small periods in the presence of a strong SC field, or at large periods with negligible SC field. However, the impact of the SC field component between electrons and ionized EL2 centres on carrier transport is very different for various excitation levels, and is expected to diminish with excitation if the photocarrier concentration significantly exceeds the concentration of deep traps [2]. Therefore, the exposure characteristics are expected to be very informative especially if measured at longer delays of the probe beam when a deep-trap assisted electrical field component is already established.

4.2. Exposure characteristics

In order to elaborate the influence of the EL2$^+$ states to non-equilibrium carrier recombination and transport, we have modelled the dependence of all charges and the SC field as a function of light intensity at various delay times and grating periods. In figure 3(a), the average concentration of EL2$^+$ centres (zeroth Fourier component of their spatial distribution) is shown as a function of light intensity. At relatively low excitations (<3 μJ cm^{-2} ps^{-1}), the EL2$^+$ concentration increases linearly with excitation and barely depends on the delay time Δt, thus revealing linear electron generation from EL2^0 states. The generation of holes is much less effective due to the small number of EL2$^+$ states as well as the smaller photoionization cross-section than that of the electrons. At this stage, the electron capture by EL2$^+$ is inefficient due to the low concentration of EL2$^+$ states. At excitations above 10 μJ cm^{-2} ps^{-1}, the density of EL2$^+$ states starts to saturate during the recording of the grating, and it decreases with excitation at longer delay times. The saturation occurs due to exhaustion of deep traps as N^+/N_T approaches the $S_n/(S_n + S_p) \approx 0.8$ ratio at which the generation rates for both

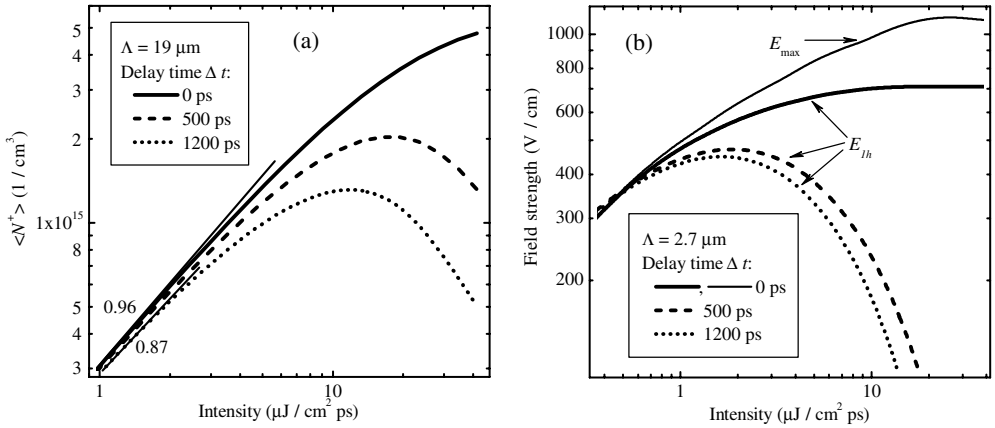

Figure 3. Calculation results shown as a function of light intensity for various delay times Δt. (a) Average concentration of ionized EL2 centres. The numbers indicate the characteristic slope coefficients of the dependences. (b) First (fundamental) harmonic of internal electric field E_{1h}. The thin solid curve shows the maximum value of the internal electric field E_{max} at $\Delta t = 0$ ps delay time.

electrons and holes from EL2 to bands become equal. Later on, the N^+ is significantly reduced by electron recombination due to the high concentration of $EL2^+$ and electrons.

Under certain experimental conditions, the recombination and transport of photocarriers may be significantly influenced by the peculiarities of the spatial profiles of $EL2^+$ and electrons. In the regime of high excitations when the saturation of N^+ takes place at the grating maxima during the photoexcitation of the carriers, the spatial profile of $EL2^+$ becomes trapezoidal. Further increase of excitation energy leads to significantly higher photocarrier concentration at the grating peaks than that of N^+, which in turn gives rise to very efficient electron recombination to the $EL2^+$ states. Generally, the effect is less pronounced in the vicinity of the grating minima. As a consequence, the spatial profile of $EL2^+$ becomes 'M' shaped with time.

In figure 3(b), we show the dependence of the first (fundamental) Fourier component of the space charge field, E_{SC}, on light intensity calculated for a $\Lambda = 2.7\ \mu$m grating period. Due to the high mobility of electrons, the SC field develops instantaneously during the process of grating recording. The amplitude of the fundamental harmonic of E_{SC} increases with excitation owing to more efficient photoionization of $EL2^0$ centres. In the regime of low excitations, until the spatial profile of $EL2^+$ remains harmonic and the generation of holes is negligible, the electron diffusion is inefficient due to the feedback of E_{SC} to the carrier transport. Thus, up to $\sim 1\ \mu$J cm^{-2} ps^{-1} the strength of the SC field barely depends on the delay time. In contrast to that, at high intensities, due to the complex spatial profile of $EL2^+$ as well as the screening of E_{SC} in the vicinity of the grating maxima, the spatial profile of E_{SC} becomes highly unharmonic, thus giving much higher E_{max} values than that of E_{1h} (see the solid curves in figure 3(b)). Moreover, at $\Delta t \geqslant 500$ ps, the SC field drops with excitation drastically. The reason for the latter effect is twofold: first, the spatial modulation of $EL2^+$ is strongly reduced due to the large concentration of electrons and their effective recombination to $EL2^+$ states (see figure 3(a)); second, as the high density of electron–hole pairs is photoexcited by EL2-assisted two-step transitions, the carrier plasma becomes capable of screening the built-in SC electric field.

Experimentally measured exposure characteristics of FC diffraction efficiency at various grating periods Λ and delay times of the probe beam Δt are shown in the upper row of figure 4.

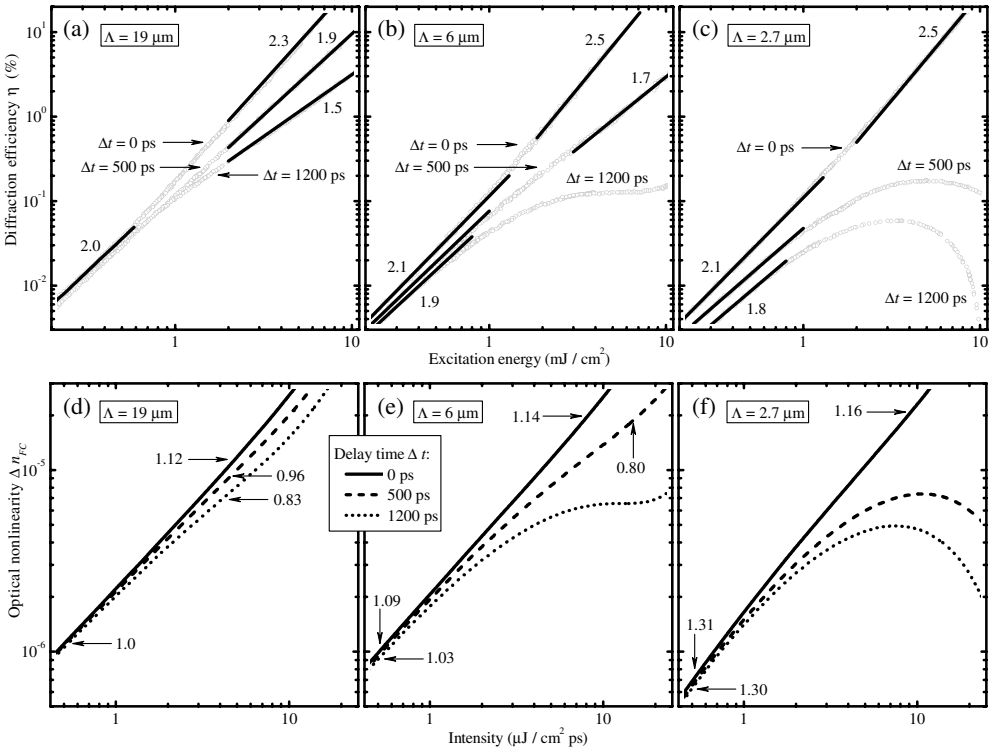

Figure 4. Experimentally measured exposure characteristics ($m = 1$) (a)–(c) and calculated free carrier optical nonlinearity as a function of light intensity (d)–(f) shown at various grating periods Λ and delay times Δt. The numbers indicate the characteristic slope coefficients of the dependences.

For comparison, the calculated free carrier optical nonlinearity as a function of light intensity is shown in the lower row of the figure. The range of intensities was chosen to cover the interval of optical nonlinearities which is most consistent with the experimental results. Because of the $\eta \propto \Delta n_{\mathrm{FC}}^2$ dependence, the characteristic slope coefficients of the calculated Δn_{FC} dependences are expected to be a factor of two lower than that of experimentally measured diffraction efficiency η.

First of all, we concentrate on experimental results at $\Delta t = 0$ ps, the most straightforward case, in order to clarify the mechanisms of carrier generation. At excitations below 1 mJ cm^{-2}, the characteristic slope of the diffraction efficiency is $\sim$2 for all grating periods, thus indicating unambiguously the monopolar generation of electrons from EL2^0. At higher excitations, the increase of the EC slope up to 2.3–2.5 is due to the fact that the EL2$^+$ concentration becomes high enough to provide a number of electron–hole pairs generated by the two-step generation process comparable to the number of electrons generated from EL2^0.

The process of EL2 recharging with excitation energy and subsequent refilling of EL2$^+$ states is most clearly evidenced at 19 μm grating period, i.e. when carrier recombination processes dominate over their diffusion. The decrease of the EC slope coefficient at high excitations with delay time is solely due to the increased number of EL2$^+$ states and electrons and their efficient recombination in the vicinity of the grating maxima, which is also confirmed by the good agreement between the calculated (figure 4(d)) and experimentally measured (figure 4(a)) dependences. On the other hand, the similarity of the experimentally measured

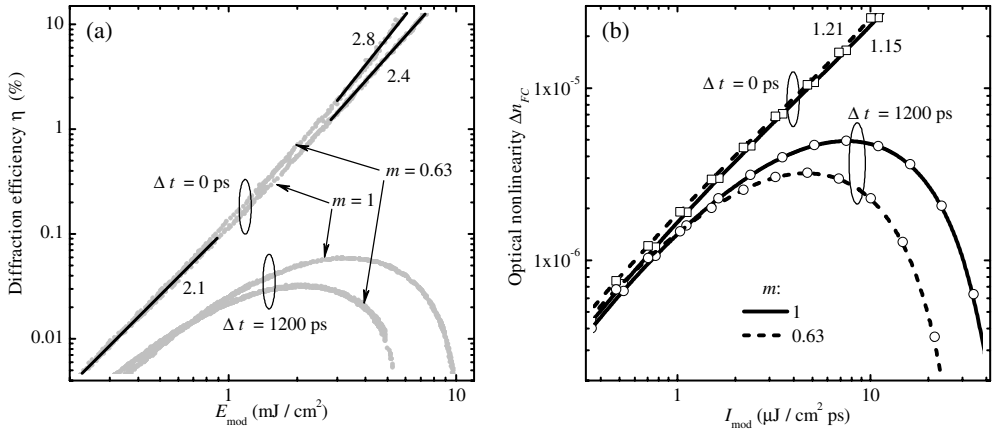

Figure 5. Experiment (a): diffraction efficiency η as a function of modulating excitation energy E_{mod} shown for two modulation depths of the interference field and two delay times of the probe beam. The thick solid curves show the fits of characteristic regions of the EC. The corresponding slope coefficients are indicated. Calculation (b): free carrier optical nonlinearity Δn_{FC} as a function of modulating intensity I_{mod} calculated for two modulation depths of the interference field and delay times of the probe beam. The numbers indicate the characteristic slope coefficients of the exposure characteristics. The grating period is 2.7 μm for both experiment and calculation.

and calculated dependences at 2.7 μm grating period points to SC-limited electron grating decay: at high excitations (above 3 mJ cm^{-2}) and $\Delta t \geqslant 500$ ps, the diffraction efficiency drops with intensity because of the reduction of EL2$^+$ modulation as well as the screening effects which lead to efficient decrease of the SC field and redistribution of electrons.

The extent to which these mechanisms influence the SC field can be controlled experimentally by varying the modulation depth m of the interference field, as an unmodulated part of the interference field causes a spatially homogeneous recharging of EL2 centres and generation of excess photocarriers. In figure 5(a), we show the experimentally measured exposure characteristics of the FC diffraction efficiency at 2.7 μm grating period and two delay times of the probe beam with modulation depth of the interference pattern set to 1 and 0.63. The diffraction efficiency is shown as a function of modulating energy of the interference field since only the modulated part of the carrier grating can originate FC diffraction. The corresponding calculations of free carrier optical nonlinearity are shown in figure 5(b). While no drastic change in characteristic slope coefficients of the EC is observed at $\Delta t = 0$ ps, the diffraction efficiency in figure 5(a) and optical nonlinearity in figure 5(b) saturate with excitation at $\Delta t = 1.2$ ns and start to decrease at higher excitations. The saturation occurs at lower excitations if m is reduced from 1 to 0.63. The effect is initiated by the unmodulated part of the interference field which leads to more effective EL2 photoionization during the carrier photogeneration process and also to the optimal two-step generation of electron–hole pairs through the EL2 centres. Moreover, the electron recombination rate is higher due to the relatively higher concentration of electrons and EL2$^+$ states. As a consequence, the SC field component between EL2$^+$ and electrons saturates and starts to decrease at lower excitations than that in the case of $m = 1$.

5. Conclusions

The exposure characteristics of light diffraction can be employed as a particularly sensitive way to study carrier recombination and transport in photorefractive semiconductor crystals.

A ps-DFWM technique has been used to investigate directly the dynamics of free carrier gratings as a function of time and excitation energy, whereas the SC field was monitored through its feedback effect to carrier transport. The exposure characteristics in GaAs:EL2 at different delay times of the probe beam and modulation depths of the interference pattern allowed us to characterize very sensitively the regimes of carrier generation, recombination, and transport through the changes in the characteristic slope coefficients of the EC. The comparison of calculations with the experimental data revealed the origin of the SC field and pointed out the mechanisms of carrier generation from/via EL2 centres and the subsequent recharging of the deep traps. The space–charge-limited electron grating decay at low excitations has been shown to change in a pure diffusive grating decay at higher excitations due to SC field screening by carrier plasma and efficient reduction of a spatial charge modulation in deep EL2 traps due to carrier recombination.

Acknowledgments

The research was sponsored by NATO Scientific Affairs Division in the framework of the Science for Peace Programme (Project SfP-974476) and Lithuanian State Science and Studies Foundation.

References

[1] Smirl A L, Valley G C, Bohnert K M and Boggess T F 1988 *IEEE J. Quantum Electron.* **24** 289
[2] Sudzius M, Aleksiejunas R, Jarasiunas K, Verstraeten D and Launay J C 2003 *Semicond. Sci. Technol.* **18** 367
[3] Jain R K and Klein M B 1983 Degenerate four-wave mixing in semiconductors *Optical Phase Conjugation* ed R A Fischer (New York: Academic) p 307
[4] Eichler H J, Günter P and Pohl D W 1986 *Laser-Induced Dynamic Gratings* (*Springer Series in Optical Sciences* vol 50) (Berlin: Springer)
[5] Baraff G A and Schluter M A 1992 *Phys. Rev.* B **45** 8300
[6] Jaraši ̄unas K and Gerritsen H J 1978 *Appl. Phys. Lett.* **33** 190
[7] Petrovic M S, Suchocki A, Powell R C, Cantwell G and Aldridge J 1989 *J. Appl. Phys.* **66** 1359
[8] Haag H, Gilliot P, Levy R, Honerlage B, Briot O, Ruffenach-Clur S and Aulombard R L 1999 *Appl. Phys. Lett.* **74** 1436
[9] Pačebutas V, Krotkus A, Aleksiejūnas R, Sūdžius M, Jaraši ̄unas K, Leszczynski M, Perlin P and Suski T 2002 *Physics of Semiconductors 2002* ed A R Long and J H Davies (Bristol: Institute of Physics Publishing)
[10] Jaraši ̄unas K and Vaitkus J 1977 *Phys. Status Solidi* a **44** 793
[11] Jaraši ̄unas K, Delaye P and Roosen G 1993 *Phys. Status Solidi* b **175** 445
[12] Sūdžius M, Bastys A and Jaraši ̄unas K 1999 *Opt. Commun.* **170** 149
[13] Aleksiejunas R, Sudzius M and Jarasiunas K 2001 *Opt. Commun.* **198** 115
[14] Jarasiunas K, Bastiene L, Launay J C, Delaye P and Roosen G 1999 *Semicond. Sci. Technol.* **14** 48
[15] Dabrowski J and Scheffler M 1989 *Phys. Rev.* B **40** 10391
[16] Martin G M 1981 *Appl. Phys. Lett.* **39** 747
[17] Dobrilla P and Blakemore J S 1985 *J. Appl. Phys.* **58** 208
[18] Boggess T F, Smirl A L, Moss S C, Boynd I W and van Stryland E W 1985 *IEEE J. Quantum Electron.* **21** 488
[19] Delaye P and Sugg B 1994 *Phys. Rev.* B **50** 16973
[20] Olsson A, Erskine D J, Xu Z Y, Schremer A and Tang C L 1982 *Appl. Phys. Lett.* **41** 659
[21] Dargys A and Kundrotas J 1994 *Handbook on Physical Properties of Ge, Si, GaAs and InP* (Vilnius: Science and Encyclopedia Publishers)
[22] Valley G C, Smirl A L, Klein M B, Bohnert K and Boggess T F 1986 *Opt. Lett.* **11** 647
[23] Champlin K S and Glover G H 1968 *Appl. Phys. Lett.* **12** 231